POLITECNICO DI TORINO
Repository ISTITUZIONALE

Spiral Groove Thrust Bearing Modeling with Finite Difference Method

Original
Spiral Groove Thrust Bearing Modeling with Finite Difference Method / Colombo, F., Goti, E., Lentini, L.. - 163:(2024), pp. 498-507. (5th International Conference of IFToMM Italy, IFIT 2024 Turin (ITA) September 11–13, 2024) [10.1007/978-3-031-64553-2_58].

Availability:
This version is available at: 11583/2995527 since: 2024-12-17T13:56:16Z

Publisher:
Springer Science and Business Media .

Published
DOI:10.1007/978-3-031-64553-2_58

Terms of use:

This article is made available under terms and conditions as specified in the corresponding bibliographic description in the repository

Publisher copyright
Springer postprint/Author's Accepted Manuscript

This version of the article has been accepted for publication, after peer review (when applicable) and is subject to Springer Nature's AM terms of use, but is not the Version of Record and does not reflect post-acceptance improvements, or any corrections. The Version of Record is available online at: http://dx.doi.org/10.1007/978-3-031-64553-2_58

(Article begins on next page)

29 November 2026

Spiral groove thrust bearing modeling with finite difference method

Federico Colombo[1], Edoardo Goti[1], Luigi Lentini[1]

[1] Politecnico di Torino, Dipartimento di Ingegneria Meccanica e Aerospaziale
federico.colombo@polito.it

Abstract. The paper aims to simulate the static load capacity of a gas spiral groove thrust bearing for a high-speed compressor. The pressure distribution inside the bearing air film is computed by discretizing and solving the Reynolds equation through a finite difference numerical scheme. The mesh convergency analysis is performed to investigate the accuracy of the solution when the number of nodes is increased inside the computational domain. The effect of the number of grooves on the load carrying capacity is also investigated while maintaining the other geometrical parameters of the bearing. The results are compared with an analytical model available in the literature.

Keywords: finite difference technique, spiral groove thrust bearing, dynamic gas bearings, high-speed turbomachinery.

1 Introduction

High-speed small-scale turbomachinery is a challenging sector in which dynamic gas bearings can be successfully employed for their characteristics of being with low friction, no wear and oil free. The actual trend in the reduction of the size of such systems is aimed at increasing the power density with a resulting increase of the rotational speeds. An overview of gas turbines in the millimeter size range is given in [1]; they may find application in small portable electronics that requires compact energy supplies. The review discusses propulsion and power applications such as combined cycles, turbopumps and cogeneration, focusing on microscale applications. A feasibility study of a small gas turbine generator is given in [2], where a turbine impeller of dia. 10 mm is taken into consideration. The output power is about 100 W, the compressor pressure ratio is about 3 and the rotational speed is about 870 krpm. An experimental test of the feasibility of such system has been carried out in [3], where the main components (compressor and combustor) were tested separately. A method to design high temperature Solid Oxide Fuel Cells (SOFC) coupled with a low power gas turbine is illustrated in [4] with the aim of minimizing the specific cost and maximizing the efficiency. In this case the electrical output power is below 10 kW. An oil free application for heat pumps is described in [4], when a radial compressor with impeller tip diameter of 20 mm is tested at rotational speeds up to 210 krpm.

The design of the dynamic gas bearings able to sustain such systems up to very high speeds is very challenging. Two main solutions can be adopted: the use of grooved bearings or foil bearings. The first ones [5] create a pressure distribution that sustain the rotor thanks to the pumping action of the grooves. The second ones make use of compliant metallic foils [6], [7], [8], [9] which allow to reach high rotational speeds as well, but with larger dynamic runouts of the rotor.

Concerning the modeling of grooved bearings, analytical or numerical approaches can be followed. The analytical models available in literature are based on the so-called Narrow Groove Theory (NGT), which neglects the pressure variation through the groove-ridge pair and assumes a mean pressure, with the advantage of obtaining the analytical expression for the pressure distribution [10] The NGT theory also makes it possible to calculate the dynamic coefficients of stiffness and damping of grooved bearings, as shown in [11]. Good agreement of the theory with experiments was found in [12]. The compressible Reynolds Equation (RE) is discretized using the Finite Element Method (FEM) and solved with the Newton-Raphson procedure in [13]. Analyses of grooved gas bearings with FEM schemes based on the Galerkin method were carried out in [14], [15].

In the present work the object of the study is modeling a thrust gas bearing with spiral grooves designed for a radial compressor rotating up to 200 krpm. The bearing is modelled numerically discretizing the RE with finite difference technique. This preliminary investigation provides a baseline characterization of the gas bearing of the prototype device to be used as the starting point to define the final design which would also consider the dynamic behavior of the bearings.

In Section 2 the numerical model based on the finite difference method is presented. It is also indicated how the geometry of the spiral grooves is simulated in the numerical model and how the calculation domain is defined due to symmetry. In Section 3 the results of the numerical model in terms of the load carrying capacity are compared to the results of the Muijderman's model while increasing the number of computational nodes and grooves.

2 Finite difference model

2.1 Numerical problem definition

Figure 1 shows the geometry of the spiral groove thrust bearing (SGTB) considered in this paper. Inward groove configuration is considered in this work since the pump-in design was confirmed to guarantee superior load carrying capacity compared to the other designs according to previous literature evidence [16]. Grooves edges are defined by logarithmic spiral curves [17] whose equation in polar coordinates reads as eq.1.

$$\theta = -\tan\alpha \cdot \ln\frac{r}{r_3} + \sum_{i=1}^{2K-1}\frac{a_1}{r} + \sum_{j=2}^{2K-1}\frac{a_2}{r}, \quad \Omega_{r,\theta} = \{r_2 \le r \le r_3\} \tag{1}$$

Where K is number of grooves, i are odd indices lower than K and j are even indices lower than K.

The following dimensionless quantities are also introduced to define the bearing geometry and aspect ratio: $X = \frac{a_1}{a_2}$, $Y = \frac{r_3 - r_2}{r_3 - r_1}$.

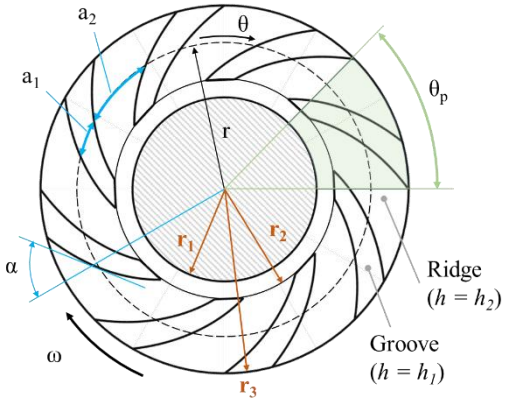

Fig. 1. Geometry parameters of a SGTB. Due to the property of the logarithmic spiral the α angle and the ratio a_1/a_2 is constant whatever the radial position between r_2 and r_3.

In this paper the RE is solved through a finite difference (FDM) scheme with mixed Dirichlet-periodic boundary conditions [18] within a computational domain that reproduces the film shape between the plates of a SGTB. Equation (2) is the static Reynolds equation in polar coordinates valid for an isoviscous, isothermal, and incompressible fluid. The assumption of isoviscous and incompressible fluids holds due to the limited pressure increase that is usually experienced by hydrodynamic gas bearings.

$$\frac{\partial}{\partial\theta}\left(\frac{h^3}{12\mu_0}\frac{\partial p}{\partial\theta}\right)+\frac{\partial}{\partial r}\left(\frac{h^3}{12\mu_0}\frac{\partial p}{\partial r}\right)=\frac{r\omega}{2}\frac{\partial h}{\partial\theta}\,, \qquad \Omega_{r,\theta}=\{0\le\theta\le\theta_p, r_1\le r\le r_3\} \tag{2}$$

where ω is the rotating speed of the moving surface w.r.t. the symmetry axis, $h = h(r,\theta)$ is the local film thickness, μ_0 is the dynamic viscosity of air ($1.81\cdot10^{-5}$ Pas), and $\theta_p = 2\pi/K$ the periodicity angle. Due to periodicity, the numerical solution is computed just within one period and periodic boundary conditions applied to reconstruct the actual pressure distribution inside the whole bearing.

For the numerical solution, it is expedient to restate the problem in dimensionless form. This limits the number of input parameters so that one numerical solution is valid for multiple dimensional problems. Scaling of variables also reduces truncation errors. The dimensionless formulation requires some reference parameters to scale the independent variables, i.e., *r*, and the dependent variables *p*, *h* of the problem. The dimensionless variables of eq. 3 are introduced in eq. 2, and the reference parameters have been selected according to eq.4. Reference parameters were chosen with the aim of simplifying as much as possible the dimensionless form of the RE. The RE reads as eq. 5 (in the following capital letters identify dimensionless quantities).

$$r_r R = r, \quad p_r P = p, \quad h_r H = h, \tag{3}$$

$$r_r = r_3, \quad h_r = h_2, \quad p_r = 6\omega r_r^2 \mu_0 / h_r^2 \tag{4}$$

$$\frac{1}{R}\frac{\partial}{\partial\theta}\left(H^3 \frac{\partial P}{\partial\theta}\right) + \frac{\partial}{\partial R}\left(H^3 R \frac{\partial P}{\partial R}\right) = R\frac{\partial H}{\partial\theta}, \quad (R,\theta) \in \overline{\Omega_{r,\theta}} = \{0 \le \theta \le \theta_p, R_1 \le R \le R_3\} \tag{5}$$

The computational domain in polar coordinates $\overline{\Omega_{r,\theta}}$ is subdivided into nodes according to a regular grid with *N* rows and *M* column, being *i* the numbering index of nodes across columns and *j* is the numbering index of nodes across rows. As to the boundary conditions (b.c.), Dirichlet boundary conditions apply to the upper and lower bounds of the domain, at $r = r_1$ and $r = r_3$, whereas periodic b.c. apply to the left and right bounds, i.e. across the θ coordinate.

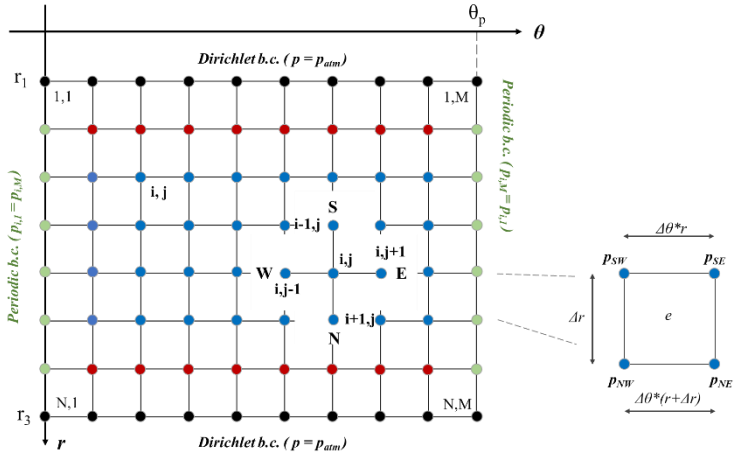

Fig. 2. Computational domain and computational stencil used to discretize the 2nd derivatives with a central difference scheme.

The numerical solution of the 2D Reynolds equation is implemented through a Finite Difference Discretization scheme (FDM). The central derivative approximation based on the computational stencil represented in Figure 2 is applied two times to each of the 2nd derivative terms at the left-hand side of the RE and once to the right-hand side.

The differential equation becomes a set of algebraic equations. The lexicographic ordering of nodes [18] allows to rewrite these algebraic equations as a linear system in the form of eq. 6 which can be solved through the Gaussian elimination method. $\boldsymbol{A}^{NMxNM}$ is eptadiagonal determining matrix, where the 1st, (N-1)th, and the Nth super-diagonals and subdiagonals are both non-zero due to the relationships between adjacent nodes of the computational grid. $\boldsymbol{P}^{NM\times 1}$ is the solution in dimensionless form (dimensionless pressure distribution).

$$\boldsymbol{A}^{NM\times NM}\,\boldsymbol{P}^{NM\times 1} = \boldsymbol{f}^{NM\times 1} \tag{6}$$

The load carrying capacity of the thrust bearing was calculated by numerical integration of the dimensional pressure distribution $\boldsymbol{p}^{NM\times 1} = \boldsymbol{P}^{NM\times 1} \cdot p_r$ across the computational domain. The area of the eth element of the grid was calculated through eq. 7, and the average of the pressure values at the nodes is associated to each element for higher accuracy (see figure 2).

$$A_e = \Delta\theta(r_e + \Delta r)\frac{(r_e + \Delta r)}{2} - (\Delta\theta r_e)\frac{r_e}{2} \tag{7}$$

$$LCC = K \cdot \sum_e A_e \frac{(p_{SW} + p_{SE} + p_{NW} + p_{NE})_e}{4} \tag{8}$$

2.2 Geometry of the thrust bearing

Dimension and operational conditions of the bearing considered in this paper are the same as those considered by the authors in [19], i.e., r_3 = 20 mm, r_1/r_3 = 0.5, h_2 = 5 μm, rotational speed ω = 200 krpm, and 6 to 20 grooves. The other geometrical parameters (i.e., *X, Y, α*, and h_1) were defined through an optimization procedure with the goal of maximizing the load carrying capacity (LCC). The NGT model by Muijderman [17] is considered here to carry out this optimization in a simplified way. Figure 3a recalls the optimized parameter thus identified and shows the related geometry. Figure 3b shows the computational domain where the stationary RE is solved in MatLab considering an upper stationary grooved surface and lower flat moving surface.

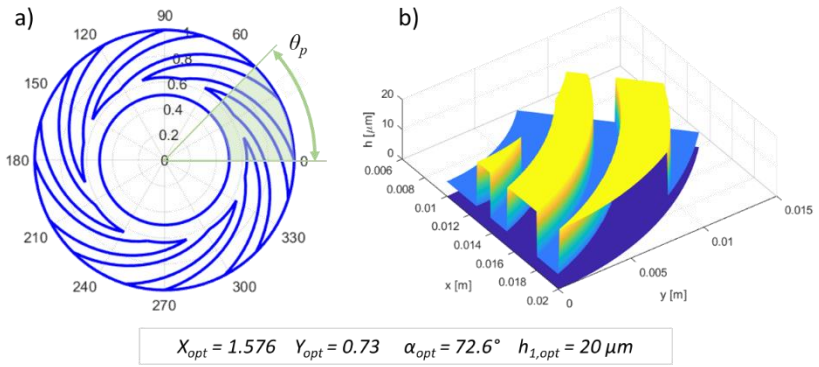

Fig. 3. Optimized geometry of the SGTB considered in this work.

Calculation of the average modified Reynolds number, as per eq. 9, in the circumferential direction suggested that the assumption of isoviscous and incompressible fluids has limiting validity for the case under investigation [18], since the condition $Re_\theta \approx 0.34 < 1$ holds but it is rather weak, because the order of magnitude is the same.

$$Re_\theta = \text{avg}\left(\frac{\rho\omega r l_{p,r}}{\mu}\left(\frac{h}{l_{p,r}}\right)^2\right) \ll 1 \tag{8}$$

where $l_{p,r}$ is the circumferential length of the symmetry domain of the bearing at radius r. Compressible RE should be considered in the future for a better estimate.

3 Comparison with an analytical model

Through the results presented in the following sections the approach of solving numerically the RE in a discretized form is compared to the NGT approach by Muijderman [17]. The NGT propose to solve a modified form of the RE analytically after applying simplifying assumption. For instance, grooves and ridges are considered sufficiently narrow so that a linearized pressure distribution inside the grooves is hypothesized to simplify the solution of the derivatives terms; pressure at both ends of the grooves, i.e. ($r = r_2$) and ($r = r_3$), is constant and end effects are neglected; an infinite number of grooves is supposed, which allows to consider just the averaged flow rate in the *r*-direction (the sawtooth pressure distribution is neglected).

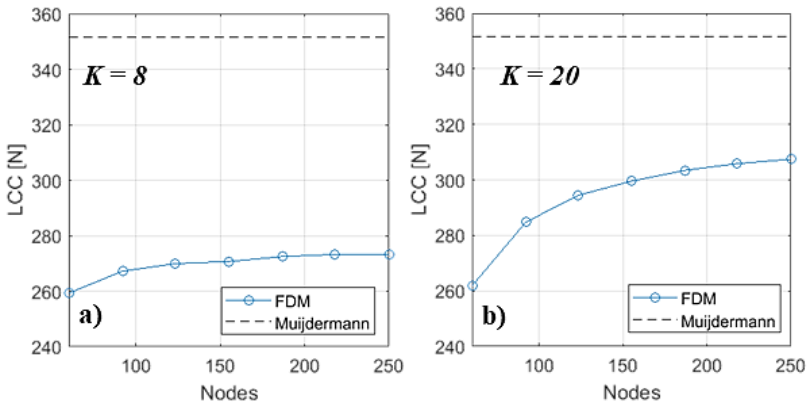

Fig. 4. Convergency of the numerical solution with increasing the density of the grid in the case with (a) 8 grooves and (b) 20 grooves.

Denser grids were not investigated since the requested memory for the calculation exceeded the available RAM installed in the PC where the simulation run (32 GB). The study was repeated two times in the case with 8 grooves and 20 grooves.

Figure 4a presents the result of the analysis with 8 grooves. It shows that using more nodes is not of interest because the solution had already reached convergency with 218 nodes. Figure 4b is the output analysis with *K = 20* and it shows that some more nodes would be necessary to reach convergency.

The results also shows that any value obtained through the numerical model is lower than the LCC estimated by Muijdermann's model. This deviation may be related to the simplifying NGT assumptions, and it will be interesting to compare these results with

experimental results from a real prototype in the future to understand how much the Muijderman's model overestimates the actual load carrying capacity of the bearing.

The computational time was also considered to identify the number of nodes to be used for the following analyses. The results suggest that one can reach up to 220 nodes with a computational time below 2'. The computation time was not affected by the number of grooves.

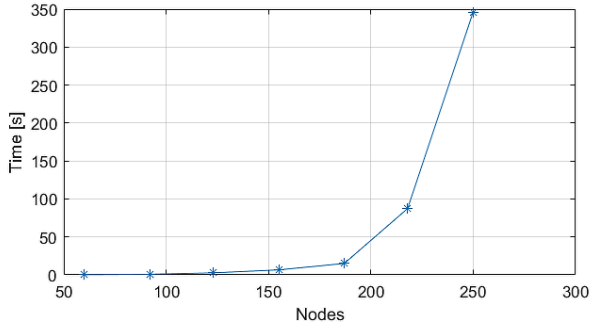

Fig. 5. Computational time with increasing the number of nodes in the case of geometry with 8 grooves.

3.1 Effect of the number of grooves

The effect of the number of grooves on the LCC was investigated more in detail by solving the numerical model iteratively while increasing the grooves from $K = 6$ up to $K = 20$. The total number of nodes was kept constant end equal to $N,M = 220$ which is a compromise to avoid overly long time for computing each iteration. As expected, the deviation between the numerical model and the NGT model reduces as the number of grooves is increased due to the hypothesis of an infinite number of grooves.

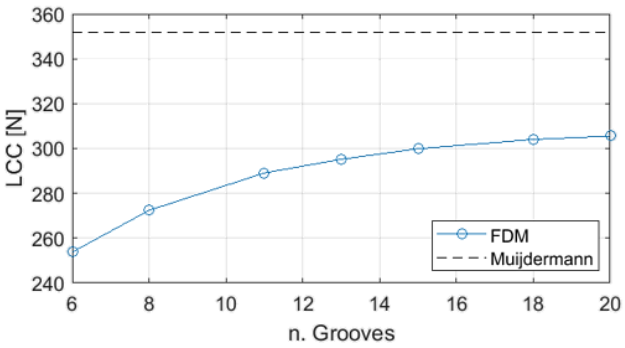

Fig. 6. Numerical solution of the RE with increasing the number of spiral grooves.

Figure 7 compares the geometry with 6, 13 and 20 grooves with same optimum geometric parameters as those of Figure 3, while Figure 6 shows that the grooves have a

considerable effect on the LCC which increases by 15% when the number of grooves is about 3 times larger.

Figure 7 also shows that when the number of grooves increases, the pressure distribution inside the thrust bearing approach a torus with a quasi-triangular section, which justifies the simplifying assumptions considered by Muijderman's model.

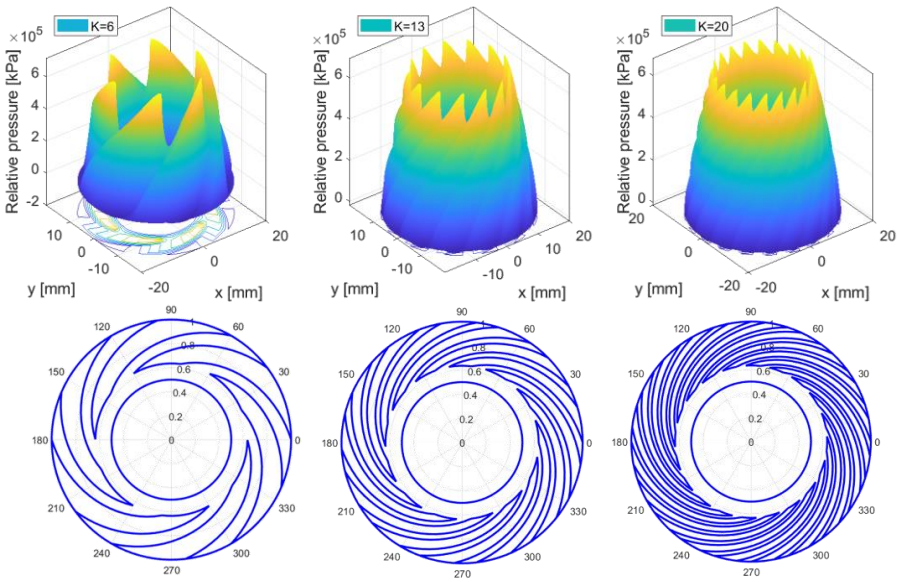

Fig. 7. Geometry and pressure distribution of a SGTB with an increasing number of grooves.

4 Conclusions

A finite difference scheme is used to discretize the dimensionless RE in polar coordinates to solve the pressure distribution inside a SGTB numerically. Optimized value of the geometrical parameters of the bearing were identified using a literature analytical model with the aim of maximizing the LCC. The same geometry was then simulated with the finite difference numerical model and the results compared.

The mesh convergency analysis indicates that the higher the number of grooves, the higher the complexity of the SGTB geometry, and, therefore, the larger is the number of nodes required into the computational grid for the numerical solution to converge. With just 8 grooves, a grid of size 220x220 nodes is enough, whereas with 20 grooves more than 250 nodes along the r-direction and θ-direction would be necessary for convergency. A lot of memory is therefore required to perform these calculations, which usually exceeds those installed in common desktop PC.

The number of grooves has an impact on the actual LCC of the bearing. Results of the numerical analysis suggest that increasing the number of grooves the thrust load the bearing is able to carry during operation is increased. This is not evidenced by analytical models of the NGT family due to the hypothesis of an infinite number of grooves which

is introduced to simplify the solution of the problem. A denser pattern of groove is probably able to pump a larger air flow inside the bearing because the ratio between grooves area and ridge area becomes probably more favorable, thus increasing the pressure build up which develops as a reaction. However, the Muijdermann's model seems to overestimate the LCC compared to the numerical model by 14% to about 25%.

In the future, the aim of the authors is to compare the results of both available analytical models and FDM with experimental analysis through dedicated test rigs to assess the limits of validity of the two approaches in the design of SGTB.

The optimization of the bearing geometry through a fully numerical strategy will also be evaluated by experiments. Numerical calculations are expected to provide a better estimate of the behavior of actual grooved dynamic bearings since the actual number of grooves is usually limited by costs and for machining reasons.

The results of static numerical simulations will be used as the starting point for implementing the numerical solution of the RE in the time domain to integrate it into the rotodynamic model of the prototype radial compressor shaft.

Acknowledgments This publication is part of the project NODES which has received funding from the MUR – M4C2 1.5 of PNRR funded by the European Union - NextGenerationEU (Grant agreement no. ECS00000036)

5 References

[1] A. H. Epstein, 'Millimeter-scale, micro-electro-mechanical systems gas turbine engines', *J. Eng. Gas Turbines Power*, vol. 126, no. 2, Art. no. 2, 2004.

[2] K. Isomura, M. Murayama, and T. Kawakubo, 'Feasibility Study of a Gas Turbine at Micro Scale', presented at the ASME Turbo Expo 2001: Power for Land, Sea, and Air, American Society of Mechanical Engineers Digital Collection, Jul. 2014. doi: 10.1115/2001-GT-0101.

[3] K. Isomura *et al.*, 'Experimental verification of the feasibility of a 100 W class micro-scale gas turbine at an impeller diameter of 10 mm', *J. Micromech. Microeng.*, vol. 16, no. 9, p. S254, Aug. 2006, doi: 10.1088/0960-1317/16/9/S13.

[4] J. Schiffmann and D. Favrat, 'Experimental investigation of a direct driven radial compressor for domestic heat pumps', *International Journal of Refrigeration*, vol. 32, no. 8, pp. 1918–1928, 2009.

[5] E. Guenat and J. Schiffmann, 'Dynamic force coefficients identification on air-lubricated herringbone grooved journal bearing', *Mechanical Systems and Signal Processing*, vol. 136, p. 106498, Feb. 2020, doi: 10.1016/j.ymssp.2019.106498.

[6] W. Luan, Y. Liu, Y. Wang, and F. Xu, 'Effect of herringbone groove structure parameters on the static performance of gas foil herringbone groove thrust bearings', *Tribology International*, vol. 177, p. 107979, Jan. 2023, doi: 10.1016/j.triboint.2022.107979.

[7] H. Li, H. Geng, X. Li, and L. Qi, 'The limiting static and dynamic performance of foil bearings', *Proceedings of the Institution of Mechanical Engineers, Part J: Journal of*

Engineering Tribology, vol. 236, no. 1, pp. 205–213, Jan. 2022, doi: 10.1177/13506501211053504.

[8] P. Samanta, N. C. Murmu, and M. M. Khonsari, 'The evolution of foil bearing technology', *Tribology International*, vol. 135, pp. 305–323, Jul. 2019, doi: 10.1016/j.triboint.2019.03.021.

[9] M. Mahner, M. Bauer, A. Lehn, and B. Schweizer, 'An experimental investigation on the influence of an assembly preload on the hysteresis, the drag torque, the lift-off speed and the thermal behavior of three-pad air foil journal bearings', *Tribology International*, vol. 137, pp. 113–126, Sep. 2019, doi: 10.1016/j.triboint.2019.02.026.

[10] 'On the Spiral Grooved, Self Acting, Gas Bearing'. Accessed: Mar. 11, 2024. [Online]. Available: https://apps.dtic.mil/sti/citations/AD0433660

[11] J. H. Vohr and C. Y. Chow, 'Characteristics of Herringbone-Grooved, Gas-Lubricated Journal Bearings', *Journal of Basic Engineering*, vol. 87, no. 3, pp. 568–576, Sep. 1965, doi: 10.1115/1.3650607.

[12] R. E. Cunningham, D. P. Fleming, and W. J. Anderson, 'Experimental Load Capacity and Power Loss of Herringbone Grooved Gas Lubricated Journal Bearings', *Journal of Lubrication Technology*, vol. 93, no. 3, pp. 415–422, Jul. 1971, doi: 10.1115/1.3451610.

[13] D. Bonneau and J. Absi, 'Analysis of Aerodynamic Journal Bearings With Small Number of Herringbone Grooves by Finite Element Method', *Journal of Tribology*, vol. 116, no. 4, pp. 698–704, Oct. 1994, doi: 10.1115/1.2927320.

[14] N. Zirkelback and L. San Andre´s, 'Effect of Frequency Excitation on Force Coefficients of Spiral Groove Gas Seals', *Journal of Tribology*, vol. 121, no. 4, pp. 853–861, Oct. 1999, doi: 10.1115/1.2834145.

[15] P. Hernandez and R. Boudet, 'Modelling of the Behaviour of Dynamical Gas Seals: Calculation with a Finite Element Method Implicitly Assuring the Continuity of Flow', *Proceedings of the Institution of Mechanical Engineers, Part J: Journal of Engineering Tribology*, vol. 209, no. 3, pp. 195–201, Sep. 1995, doi: 10.1243/PIME_PROC_1995_209_425_02.

[16] F. Colombo, E. Goti, L. Lentini, and T. Raparelli, 'Investigation on the static characteristics of a dynamic gas thrust bearing with spiral grooves for a small-scale high-speed application', vol. Proceedings of the 5th International Tribology Symposium of IFToMM, May 2024.

[17] E. A. Muijdermann, *Spiral Groove Bearings*. Springer-Verlag, 1966.

[18] A. Almqvist and F. P. Ràfols, 'Scientific Computing with Applications in Tribology: A course compendium - Luleå University of Technology'. 2019.

[19] F. Colombo, Edoardo Goti, Luigi Lentini, and Andrea Trivella, 'Optimization of a herringbone grooved thrust bearing', vol. Proceedings of the 5th International Tribology Symposium of IFToMM, May 2024.